Electronic Supplementary Material (ESI) for Environmental Science: Advances.

Supporting Information: Single-entity coccolithophore electrochemistry shows size is no guide to the degree of calcification

Minjun Yang[1], Christopher Batchelor-McAuley[1], Samuel Barton[2], Rosalind E.M. Rickaby[2], Heather A. Bouman[2], Richard G. Compton[1*]

[1] Physical and Theoretical Chemistry Laboratory, Department of Chemistry, University of Oxford, South Parks Road, Oxford OX1 3QZ, Great Britain.

[2] Department of Earth Sciences, University of Oxford, South Parks Road, Oxford OX1 3AN, Great Britain.

* corresponding author email: Richard.Compton@chem.ox.ac.uk

Contents

Section 1: Experimental

Chemicals

1,4-dihydroxybenzene (H_2BQ), calcium chloride dihydrate and potassium chloride were purchased from Sigma-Aldridge, U.K. All chemicals were used without further purification. Aqueous solutions were made using ultrapure water (Millipore, resistivity 18.2 MΩ cm at 25 °C). All solutions containing H_2BQ were freshly prepared on the day of the experiments.

Cell cultures

The cultures used in this study were obtained from Roscoff Culture Collection (RCC, France): *E. huxleyi* (RCC1216), *G. oceanica* (RCC1314) and *C. braarudii* (RCC1198). All cultures were grown on a K/2 enriched growth medium modified from the recipe for K medium with f/2 vitamins.[1] Aquil synthetic ocean water was used instead of natural seawater.[2] The final molarity of each of the medium components in the K/2 recipe are listed in Table S1.[3] To maintain the cultures, regular sub-culture inoculations were made during exponential population growth into Tissue Culture Treated Flasks (culture area 25 cm^2, 0.2µm vented cap,Corning™ Falcon™, USA), under sterile conditions, to a total culture volume of 40mL with sterile K/2 medium. The 0.2µm hydrophobic membrane on the cap of the flasks allowed for essential air exchange, whilst also protecting against microbial contamination. No additional nutrients were added to the cultures following inoculation, thus culture growth was eventually limited by the starting quotas of nutrients in the 40mL volume .All cultures were kept in a PHCbi MLR-352-PE Incubator (PHC Europe B.V.), on a 14:10 light-dark cycle with a PAR intensity of 20-40 µmol m^{-2} s^{-1}. Prior to initiating the experimental cultures, we anticipated that the circadian rhythm was synchronized for each of the cultures, as the culturing and incubation conditions described above had been maintained for >1 year beforehand, thus population cell division of each culture was likely to happen as a cohort during each dark period.[4] Electrochemistry studies of the coccolithophores were therefore conducted between 2 - 4pm each day so that the various measurements of cell morphology were obtained at roughly

the same time point in the circadian rhythm. Simultaneously, we also measured the cell numbers per mL for each experimental culture using a coulter counter (Beckman Coulter Z2 Particle Counter) so that we could track culture growth alongside measuring cellular $CaCO_3$ each day (see Figure 4 a,b,c).

Table S1. A summary of the molar concentration of all the components in the synthetic ocean water based K/2 growth medium.

		Molar Concentration in final K/2 growth medium (mol dm^{-3})
Synthetic Ocean Water (SOW) based on the Aquil medium recipe[2]	NaCl	4.20×10^{-1}
	Na_2SO_4	2.88×10^{-2}
	KCl	9.39×10^{-3}
	$NaHCO_3$	2.38×10^{-3}
	KBr	8.40×10^{-4}
	H_3BO_3	4.85×10^{-5}
	NaF	7.15×10^{-5}
	$MgCl_2.6H_2O$	5.46×10^{-2}
	$CaCl_2.2H_2O$	1.05×10^{-2}
	$SrCl_2.6H_2O$	6.38×10^{-5}
K/2 medium enrichment based on the K recipe[1], silica included	$Na_2SiO_3.9H2O$	2.52×10^{-4}
	$NaNO_3$	4.41×10^{-4}
	NH_4Cl	2.50×10^{-5}
	Na_2 b-glycerophosphate	5.00×10^{-6}
	H_2SeO_3	5.00×10^{-9}
	$Na_2EDTA.2H_2O$	5.55×10^{-5}
	$FeCl_3.6H_2O$	5.85×10^{-6}
	$MnCl_2.4H_2O$	4.50×10^{-7}
	$ZnSO_4.7H_2O$	4.00×10^{-8}
	$CoCl_2.6H_20$	2.10×10^{-8}
	$Na_2MoO_4.2H_2O$	1.30×10^{-8}
	$CuSO_4.5H_2O$	5.00×10^{-9}
F/2 vitamin enrichment[1]	Thiamine. HCl (Vitamin B1)	2.96×10^{-7}
	Biotin (Vitamin H)	2.05×10^{-9}
	Cyanocobalamin (Vitamin B12)	3.69×10^{-10}

Microscopy imaging and image analysis

Scanning electron microscopy

Phytoplankton cultures were filtered using a polycarbonate filter (3.0 μm), washed with deionized water, and subsequently dried at atmospheric pressure. Prior to the imaging, a thin layer of gold was coated over the filtered sample using a rotary pumped coater (Q150RES, Quorum, UK). The Scanning Electron Microscopy (SEM) images and Energy-dispersive X-ray

(EDX) spectroscopy were obtained using a Sigma 300 FEG-SEM from Zeiss with an accelerating voltage of 10.0 kV.

Optical microscopy

Optical measurements were made on a Zeiss Axio Examiner, A1 Epifluorescence microscope (Carl Zeiss Ltd., Cambridge U.K.), using a 20x objective lens (NA = 0.5, EC Plan-Neofluar) for *E. huxleyi* and *G. oceanica* and 10x objective lens (NA = 0.3, EC Plan-Neofluar) for *C. braarudii*. The video acquisition was provided by a Hamamatsu ORCA-Flash 4.0 digital CMOS camera (Hamamatsu, Japan), providing 16-bit images with 4-megapixel resolution.

Opto-electrochemistry apparatus

The 3D-printed (Form 2, Formlabs, UK) opto-electrochemical cell houses a three-electrode setup: a glassy carbon electrode (diameter = 3.00 mm, BASi, USA) as the working electrode, a saturated calomel electrode (SCE, ALS distributed by BASi, Tokyo, Japan) was used as the reference electrode and a graphite carbon rod as the counter electrode. Approximately 50 µL of culture sample containing the coccolithophores were dropcasted onto the glassy carbon electrode prior to the experiment. A period of time of approximately 30 s was allowed for the coccolithophores to sediment onto the surface of the electrode before the culturing solution were adsorbed carefully by tissue. The opto-electrochemical cell is then filled with ~1.0 ml of electrolyte containing 0.7 M KCl, 20 mM $CaCl_2$ and either 2 or 10 mM of H_2BQ. A higher concentration of the acid-precursor is used for *C. braarudii* (10 mM of H_2BQ) and 2 mM is used for *G. oceanica* and *E. huxleyi*. Potentiostatic control and synchronization with the microscopy camera were provided by a previously developed in-house built device[5] and current amplifier (Keithley 427) from Keithley Instruments Inc, US. A potential of +1.0V vs SCE was applied to the working electrode to drive fully the oxidation reaction of hydroquinone to form benzoquinone and two molar equivalents of protons.[3]

The opto-electrochemical experiments require approximately 5 minutes from setup to completion. This includes: injecting coccolithophore samples into the opto-electrochemical cell, setting up the optical focus for imaging, connecting the electrodes to the potentiostat and the time required for the electro-generated acid to completely dissolve pico- to nano- grams of biogenic calcium carbonate. Depending on the number density of the coccolithophore sample, which varies between species and incubation period, typically 10-50 individual coccolithophore were analysed per opto-electrochemical experiment.

Image analysis

During the course of the opto-electrochemical experiment the cell was optically imaged at 10 fps. The resulting series of images were analyzed using (Fiji distribution) ImageJ freeware.[6] Macro scripting in ImageJ allows *living* coccolithophore individuals to be identified and separated from inanimate shrapnel by their *in vivo* chl-a fluorescence signals. Coccolithophores that are within a distance of five coccosphere radii are removed from the analysis, see below for acid dissolution kinetics of coccolithophores. The stack of images containing the individual coccospheres was auto-thresholded by built-in imageJ methods to extract the projection area in the 2-D image plane. The image analysis to calculate the PIC and POC of all individual coccolithophores present in an experiment requires approximately 4-5minutes and this can be executed in parallel to the experiments.

Section 2: Energy-dispersive X-ray spectroscopy of coccolithophores

Figure S1 shows SEM images of *C. braarudii, G. oceanica* and *E. huxleyi* after 9 days of growth. The white rectangles represent the region of interest in which the energy-dispersive X-ray (EDX) spectrums were sampled. The ratio of the elements is shown in the inlay of the EDX spectrum. The elemental mapping reports carbon (~35%), oxygen (~53%), calcium (~10%) and other trace elements such as sodium and chloride which may arise from residues of the culture medium. EDX reveals a higher atomic ratio of carbon and oxygen to the amount of calcium expected for pure $CaCO_3$. This is likely due to the polysaccharide layer present on the surface of the biogenic coccoliths.[7] Note that the EDX reported ratio of Ca:C:O is likely *not* representative of the entire coccosphere because the ray penetration is typically only microns below the surface of dense materials. The mass percentage of polysaccharides on *E. huxleyi* and *G. oceanica* coccoliths are reported to be no more than 3%.[8] Assuming that all calcium is $CaCO_3$, the remainder carbon and oxygen atom% associated with the polysaccharide layer is approximately 1:1 which is in full consistence with the molecular formula of common polysaccharide units such as glucose, fructose and mannose ($C_6H_{12}O_6$).

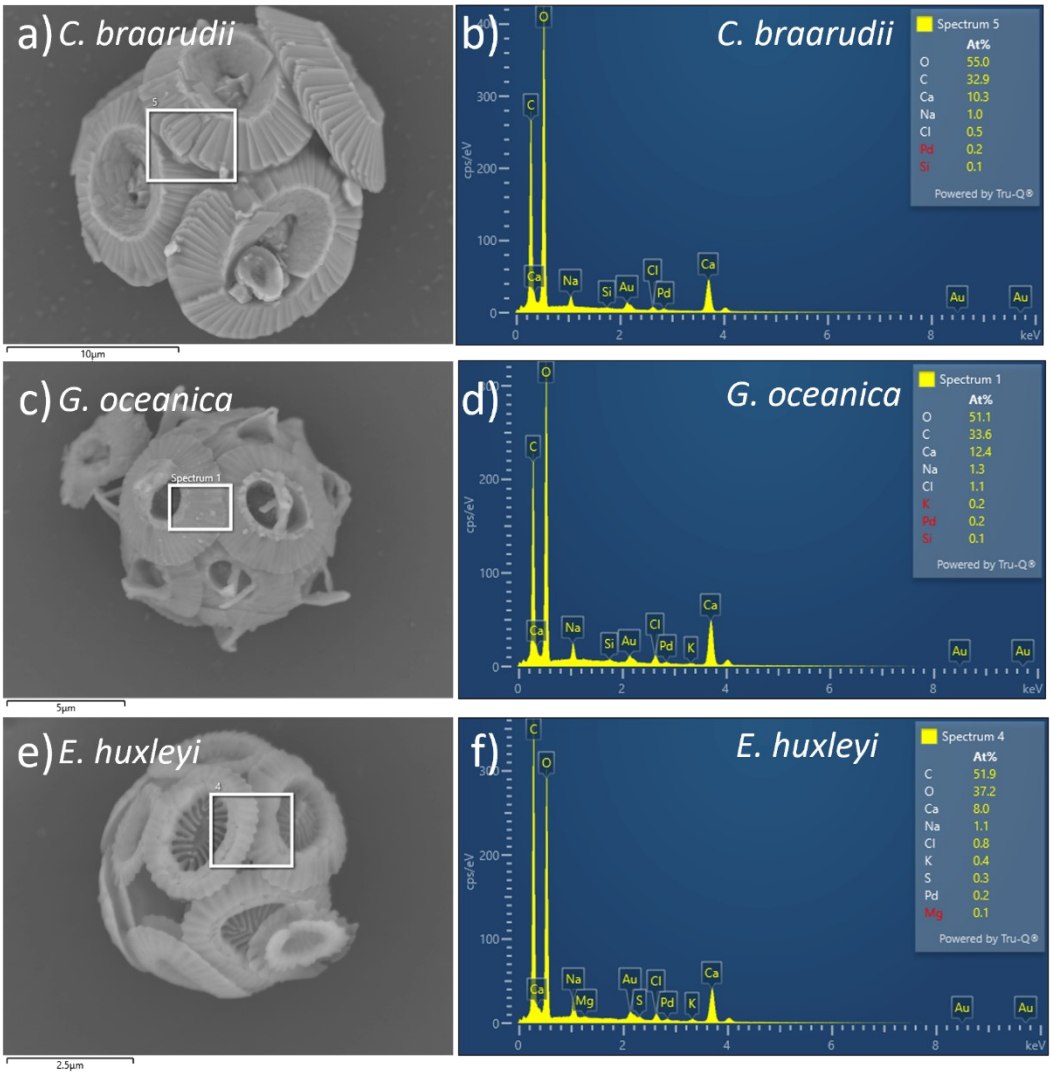

Figure S1. Elemental analysis of C. braarudii, G. oceanica and E. huxleyi coccosphere. a, c and e) are SEM images of the coccolithophore. Scale bar can be found at the bottom-left of each of the images. b), d) and f) shows the EDX spectrum and the element distributions. The region of the EDX integration is represented by the white rectangle shown in the corresponding SEM image.

Section 3: Dissolution of coccospheres in Ca^{2+}-free electrolyte

The solubility constant (K^0_{sp}) of calcite, $CaCO_3$, in infinite dilution at 298K is 3.3×10^{-9} M^2.[9]

$$CaCO_3(s) \rightleftharpoons Ca^{2+}(aq) + CO_3^{2-}(aq); \; K_{SP} = [Ca^{2+}][CO_3^{2-}] \qquad \textit{Equation S1}$$

In seawater, however, the solubility of calcite changes as a function of temperature (K) and salinity (g/kg, ‰)[9]:

$$\log\left(K^*_{sp}\right) = \log\left(K^0_{sp}\right) + \left(- 0.77712 + 0.0028426T + \frac{178.34}{T}\right)S^{0.5} - 0.07711S + 0.0041249S^{1.5} \qquad \textit{Equation S2}$$

Using a typical seawater salinity of ~ 30‰, the solubility of calcite K^*_{sp} in seawater at 298K can be calculated using Equation S2 to give a value of 3.5×10^{-7} M^2. This suggests a solution saturated with $CaCO_3$ will contain ~0.6 mM of Ca^{2+} and CO_3^{2-}. Figure S2 shows the optically measured size of individual coccolithophores as a function of time in electrolytes containing various saturation levels of Ca^{2+} and CO_3^{2-}. Each line represents a single/individual coccolithophore cell. As can be seen in Figure S2 a), the size of the *E. huxleyi* coccospheres were invariant over 6 minutes in the culture medium, which contains an over-saturation of 2.4 mM of HCO_3^- and 10 mM of Ca^{2+} (See Table S1). The radius of *E. huxleyi* coccospheres spans over the size range of 3.2 – 3.9 μm. This is not surprising because coccolithophores grow in the K/2 culture medium which mimics sea-water conditions, more of which see SI Section 1. Moving away from the culture medium, in a solution containing 0.7M KCl and 10mM of Ca^{2+} and HCO_3^- (oversaturated with respect to calcite), the size of the coccolithophores were also invariant over the timescale of the experiment. Next, removing the HCO_3^-/CO_3^{2-} components to leave a solution containing only 10 mM of Ca^{2+} and 0.7M KCl, as shown in Figure S2 c), is sufficient to prevent the dissolution of the calcareous shell over the time of the experiment. In the ***absence*** of neither Ca^{2+} *nor* HCO_3^-, however, the coccolithophore radius decreased by approximately 0.5 μm over the time scale of a few minutes. It is clear that this corresponds to

the dissolution of the biogenic calcite shell of the *E. huxleyi* coccolithophores in an under-saturated solution with respect to $CaCO_3$. Moreover, Figure S3 plots the size of the individual coccolithophores measured optically in the opto-electrochemical experiment, before and after, complete acid dissolution ***in the absence*** of added Ca^{2+}. As can be seen, the *E. huxleyi* and *G. oceanica* coccosphere at the early part of the growth curve lie on the y = x line which corresponds to no shell at the time of the opto-electrochemical measurement (invariant to acid attack). This is because the time required to set up the opto-electrochemical experiment, which is approximately 3 minutes after the addition of Ca^{2+}-free electrolyte, the calcareous shell is already dissolved. Therefore, it is essential to conduct the opto-electrochemical experiments with the addition of *at least* 10mM of Ca^{2+} in the electrolyte. Note that HCO_3^- is not added as shown herein that, first, it is not essential, and two, it will prohibit the acid dissolution of calcite as HCO_3^- is a buffer and reacts with the electrogenerated protons.

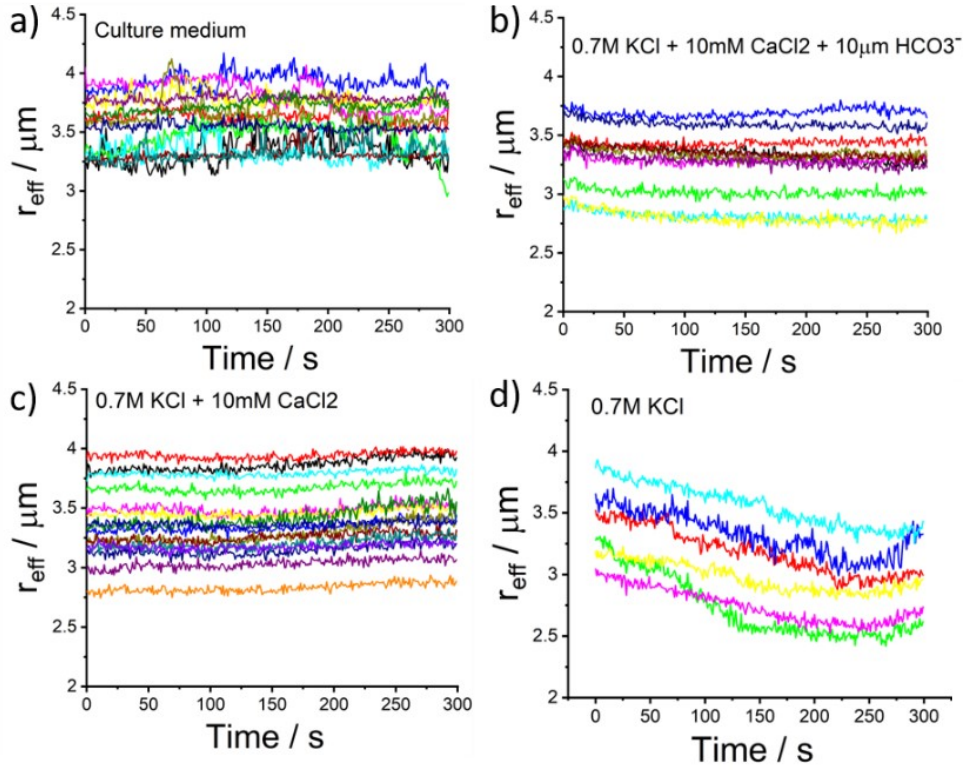

*Figure S2. Optical sizing of E. huxleyi coccospheres as a function of time immersed in different compositions of aqueous electrolytes: **a**) K/2 culture medium, **b**) 0.7M KCl, 10mM $CaCl_2$ and 10µM $NaHCO_3$, **c**) 0.7M KCl and 10mM $CaCl_2$ and **d**) 0.7M KCl only. In all cases, approximately 30s is required to set to the image acquisition after exposing the coccolithophore to the electrolyte. Each line represents an individual coccolithophore.*

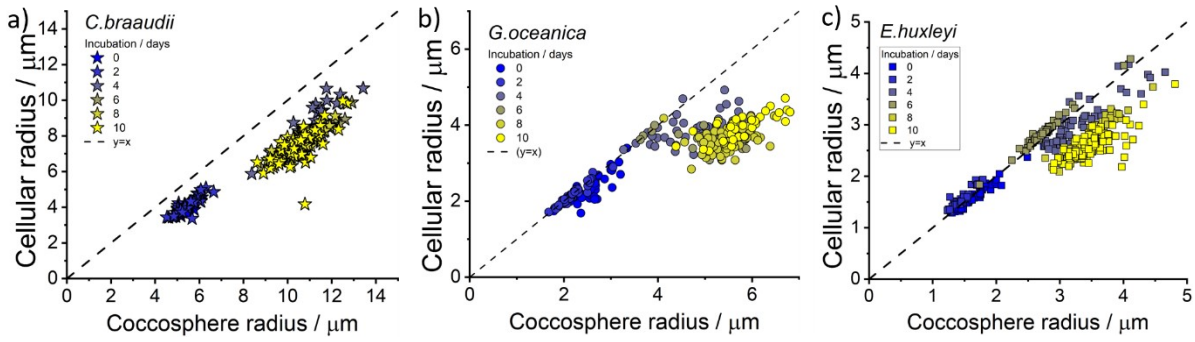

Figure S3. The effective radius of coccolithophores measured after complete acid dissolution against that prior to acid dissolution. Speciation of coccolithophores: a) C. braarudii, b) G. oceanica and c) E. huxleyi. The electrolyte contains 0.7M KCl and either 10mM of H_2BQ for C. braarudii or 2mM H_2BQ for G. oceanica and E. huxleyi. The dotted line represents the y=x line corresponding to no $CaCO_3$ shell.

Section 4: Acid dissolution kinetics of core-shell particles: theory

In this section, we consider the rate at which the calcite in a coccolithophore is expected to dissolve when the coccosphere is supported on an acid-producing electrode substrate. The electrode produces acid by oxidising hydroquionone (^{H_2}BQ) to benzoquinone (BQ) as given by:

$$H_2BQ(aq) \rightarrow BQ(aq) + 2H^+(aq) + 2e^- \qquad \textit{Equation S3}$$

This locally formed acid diffuses outward and reacts with the biogenic calcite, as described by the following reaction:

$$CaCO_3(s) + 2H^+(aq) \rightarrow Ca^{2+}(aq) + CO_2(g) + H_2O(l) \qquad \textit{Equation S4}$$

In the following, we will consider the coccolithophore to be a perfect sphere and determine the mass-transport limited flux to it.

Mass-transport controlled flux to a sphere on a generator

For a sphere isolated in the solution phase the diffusion only mass-transport limited flux (j/ mol s^{-1}) to the surface of the sphere is:[10]

$$j_{MT} = 4\pi rDC\left(\frac{r}{(D\pi t)^{0.5}} + 1\right) \qquad \textit{Equation S5}$$

At short times the flux to the surface is proportional to the surface area of the particle and at long times a steady-state is attained where the rate is proportional to the radius of the particle. Importantly for the present case when the sphere is supported on a planar surface, and hence the surface diffusionally blocks material from reaching the particle, then the steady-state flux ($j_{MT, ss}$) to the particle in the long-time limit is an analytically tractable problem[11], where:

$$j_{MT, ss} = 4\pi rDC\ln(2) \qquad \textit{Equation S6}$$

The presence of the supporting surface decreases the diffusional mass-transport limited flux by *ca.* 30% as compared to a sphere isolated in the solution (1-ln(2)).

For the experimental example in this work, the acid is not present in the bulk solution but is generated electrochemically from an acid precursor at the electrode surface. Hence, we can think of the electrode as a generator of, and particle being a 'collector', of protons.

In the following, we consider the case where at the electrode, species A (hydrobenzoquinone) is converted into two stoichiometric equivalents of B (protons).

$$A \rightarrow 2B \qquad \textit{Equation S7}$$

Species B diffuse down the concentration gradient away from the electrode surface and is subsequently irreversibly consumed at the surface of the calcite particle according to Equation S4. In this model we only need to consider the mass-transport of two species, A and B. Figure S4 schematically summarises the problem to be solved:

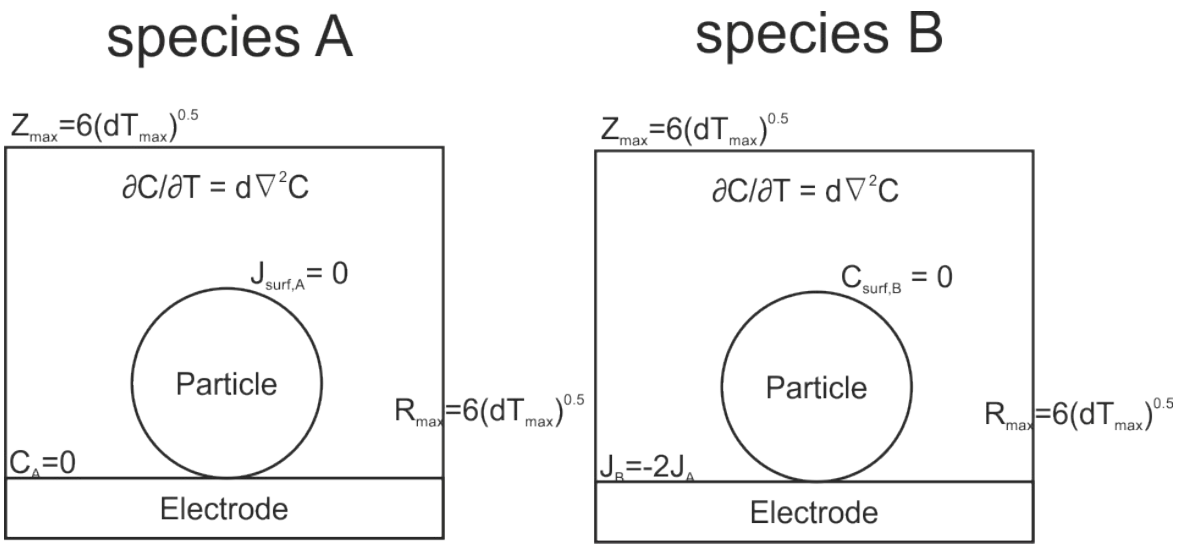

Figure S4: Schematic of the mass-transport problem that requires solving for a slowly dissolving spherical particle on a generating plate (electrode). Initially, species A is uniformly distributed across the solution phase and species B is not present. Nomenclature follows that used in ref.[12]

Initially, the concentration of species A is uniform across the solution phase and there is no species B present. After the electrode is 'switched-on' species A is then consumed at a mass-transport limited rate at the electrode surface to form two stoichiometric equivalents of B. Species B then diffuses out from the electrode and is itself irreversibly and instantaneously consumed at the particle surface. The model contains separate variables to account for unequal diffusion coefficients of species A and B. Due to the symmetry of the system, and through the

use of a cylindrical coordinate system, the problem can be reduced to two-dimensions. Solving this generator-collector problem requires numerical simulation. Herein we use a fully implicit central finite difference scheme[12] to solve the diffusion equation subject to the boundary conditions outlined in Figure S4. Numerical solving of the resulting system of simultaneous equations was achieved using a GPU optimised iterative solver[13, 14] method allowing the fully implicit two-dimensional problem to be solved without recourse to the use of explicit terms as used for example in the ADI method.

There are two important questions that can be answered by this numerical model a) does the flux to the sphere reach a steady-state and if so on what timescale and b) if a steady-state flux is attained what controls the magnitude of the flux. Figure S5 presents the numerically calculated concentration profiles for species A and B at three different times where the diffusion coefficients of species A and B are equal.

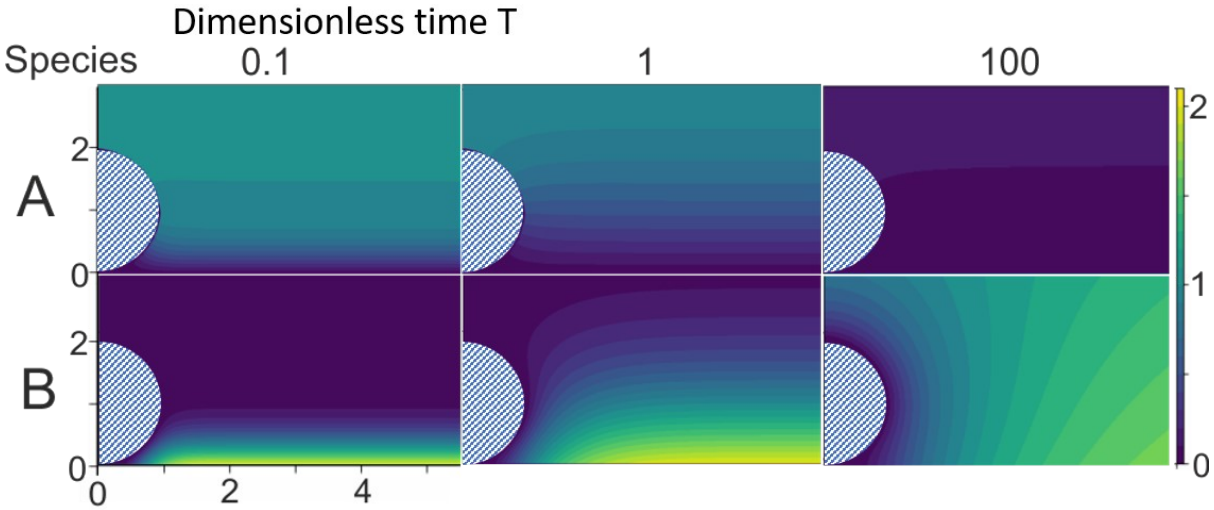

Figure S5. Concentration profiles for both species A (top row) and B (bottom row) for a particle on a generating plate for three different times. Initially, species A is uniformly present in the solution phase at a concentration of 1, and there is no B. Species A is subsequently converted to species B (at the electrode, x-axis) at a diffusion-limited rate. Following the stoichiometry of the reaction, two B are produced per A. Hence at the electrode surface at short times the concentration of the B is 2. B subsequently diffuses away from the interface and is consumed irreversibly and instantaneously at the surface of the spherical particle. Note both the x- and y-axis are normalised to the size of the particle, where the particle has a radius of 1.

In this figure only half of the particle is shown, further, the x and y coordinates are normalised to the size of the particle where the particle has a radius of one. The time is also presented in its dimensionless form, $T = Dt/r^2$. At short times ($T = 0.1$) the diffusion layer is small as

compared to the size of the particle. As T increases the diffusion layer expands and species B is consumed at the particle surface. Integration of the flux of B across the particle surface allows the flux to the particle to be numerically assessed as a function of time.

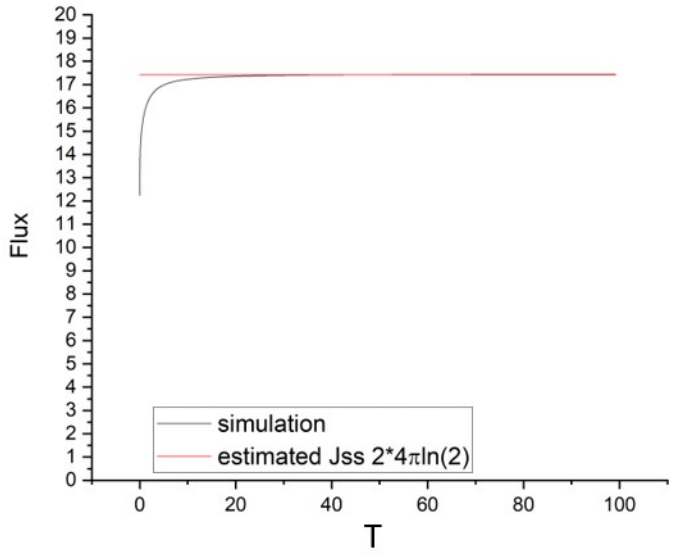

Figure S6. A plot of the numerically calculated flux to the spherical particle on the generating electrode. As B is not initially present in the solution phase at very short times the flux of B to the particle is close to zero, before rising and after T ≈ 1 reaching a steady-state flux.

Figure S6 presents the dimensionless flux (=j/DCr) of B to the particle as a function of the dimensionless time (T). At short times the flux of B to the particle is low and increases as the diffusion layer of B expands. At long times (T >20) a steady-state flux of B to the particle arises, moreover this steady-state is rapidly attained where even at T = 1, the flux is within 10% of its steady-state value. For example, for a particle with a 10 micron radius we would predict that the flux to the sphere will be within 10% of its steady-state value after only ~0.1 seconds. Furthermore, in the case where the diffusion coefficient of species A is equal to B then the steady-state dimensionless flux of B to the particle surface is found to be 17.4. Analytically this steady-state flux is equal to $\chi 4\pi\ln(2)$, where χ is the stoichiometric ratio between species A and B, i.e. for the present model this value is 2. Hence, the steady-state flux to the spherical particle on a generating electrode is the same as the flux to a sphere on a surface bathed in a bulk solution of B, where the concentration of B is double that of A! All that needs to be considered now is how unequal diffusion coefficients of species A and B will influence the

flux of B to the particle surface. Succinctly stated the flux to the particle is proportional to the square root of the product of the two diffusion coefficients. Consequently, at steady-state the flux (j /mol s^{-1}) of species B to the particle in its dimensional version, where B is generated at the supporting electrode is, reported for the first time:

$$j_{MT} = \chi 4\pi \ln(2)(D_A D_B)^{0.5} c_{A,bulk} r_{sphere} \qquad \textit{Equation S8}$$

where for the present case χ equals 2, reflecting the stoichiometry of the electrode reaction. In the main body of the text, this expression is used to describe the mass-transport limited flux of protons to the coccolithophore.

Section 5: Uncertainty in PIC measurements

In this section, the uncertainties associated with both the measurement leading to, and the calculation of, PIC are discussed. In particular, first, experimentally, the error associated with the optical sizing of particles is compared to that obtained under SEM imaging. Second, for the calculation of PIC an estimated value of the surface roughness factor (R_f) is used and how much of this uncertainty affects the PIC content.

Particle sizing measurements: optical imaging versus SEM

Figure S7 shows a direct comparison of the same *E. huxleyi* sample taken by SEM and optical microscopy. The region of interests outlined in yellow was obtained after image thresholding. The outlined area is used to calculate the effective particle radius (r_{eff}) assuming a perfect sphere (area = πr_{eff}^2). Table S2 summarises the size difference between SEM and optical images of the same coccolithophore individuals. As can be seen, optical measurements have the tendency to overestimate r_{eff} by up to 20% relative to that obtained via SEM imaging. This overestimation in the optical size measurements is due to the limitation in the wavelength of light (~400 nm) resulting in a blurred edge of the particle. Note that this is an intrinsic limitation of optical techniques for sizing micron-sized particles. No correction for optical measurement of r_{eff} was made for PIC and POC calculations.

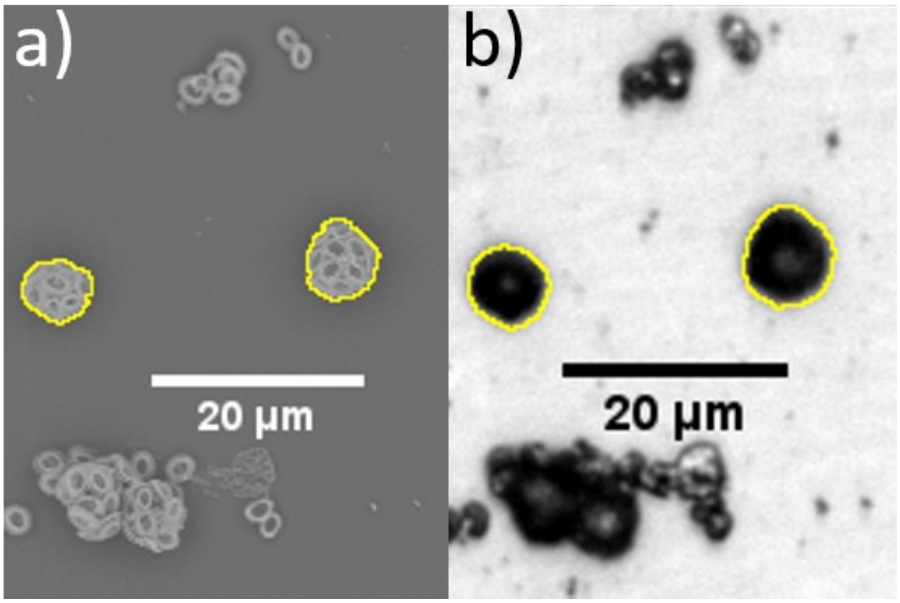

Figure S7. Identical E. huxleyi coccolithophores imaged using a) SEM and b) optical microscope with a 20x obj. lens. The yellow outline is used to calculate the projection area of the coccosphere, statistics of which are displayed in Table S2. Scale bar = 20µm.

Table S2. The effective radius of identical coccospheres measured in SEM and optical aquired images. The effective radius is the radius of a perfect circle with the equivalent area, $r_{eff} = (area/\pi)^{0.5}$. For the optical measurements, 10x objective lens is used for C. braarudii and 20x is used for G. oceanica and E. huxleyi.

Species	***Sample size***	***r_{eff} (SEM) / µm***	***r_{eff} (optics) / µm***	***Over-estimation by optics / µm***	***Over-estimation by optics in %***
C. braarudii	*11*	*10.7±1.0*	*10.9±1.1*	*0.2*	*+1.8%*
G. oceanica	*4*	*5.0±0.3*	*5.9±0.3*	*0.9*	*+18.0%*
E. huxleyi	*8*	*3.2±0.3*	*3.9±0.4*	*0.7*	*+21.8%*

Effects of surface roughness factor (R_f)

The dissolution of coccolithophores (r_{eff} ~ 10 µm) under strong acid conditions occurs in a mixed kinetics regime as discussed in the main text. The total flux of acid reacting away from the calcareous shell, j_{tot} (mol s^{-1}), is the reciprocal of the sum of the reciprocal of j_{surf} and j_{MT}. Where the surface-limited reaction kinetics, j_{surf}, is directly proportional to the surface roughness factor (R_f). Note that R_f is related to the specific surface area of a sphere by

$$Area = 4\pi R_f r^2$$

The R_f value of a standard golf ball, accounting for the area of the dimples, is approximately ~1.3. Therefore, it is not unreasonable that a coccosphere, encrusted with inter-locking coccoliths, may have R_f values ranging from 2 – 6. The PIC values reported in the main text are calculated assuming an R_f value of 4. Separately provided pdf, more of which described in SI Section 6, tabulates the calculated PIC masses of coccolithophores using different values of R_f (=2, 4 and 6). For *C. braarudii*, the PIC mass calculated using $R_f = 4 \pm 2$ gives an average value of 3.9 ng $\pm {}^{9}_{20}\%$. For *E. huxleyi*, the effect of uncertainty of R_f is larger resulting in an average PIC mass of 26 pg $\pm {}^{19}_{32}\%$. Note that due to the difference in the r_{eff} proportionality for j_{surf} and j_{MT} (Equation 3), the calculated PIC mass has a larger uncertainty for smaller sized coccospheres as a result of the estimated R_f.

Section 6: Single-entity data

Individual coccosphere data obtained in the opto-electrochemical experiment can be found in the pdf file attached separately. The table includes the effective radius (μm) of the coccosphere before and after complete acid dissolution, the time (s) taken to dissolve the calcareous shell and the calculated $CaCO_3$ mass (g) of each coccolithophore using R_f = 2, 4 and 6. Note that neighbouring coccolithophores within a proximity of 5 coccosphere radii are excluded from the analysis.

References

1. M. D. Keller, R. C. Selvin, W. Claus and R. R. Guillard, *Journal of Phycology*, 1987, 23, 633-638.
2. F. M. Morel, J. Rueter, D. M. Anderson and R. Guillard, *Journal of Phycology*, 1979, 15, 135-141.
3. M. Yang, C. Batchelor-McAuley, S. Barton, R. E. M. Rickaby, H. A. Bouman and R. G. Compton, *Angewandte Chemie*, 2021, 133, 21167-21174.
4. M. N. Müller, A. N. Antia and J. LaRoche, *Limnology and Oceanography*, 2008, 53, 506-512.
5. C. Batchelor-McAuley, J. Ellison, K. Tschulik, P. L. Hurst, R. Boldt and R. G. Compton, *Analyst*, 2015, 140, 5048-5054.
6. J. Schindelin, I. Arganda-Carreras, E. Frise, V. Kaynig, M. Longair, T. Pietzsch, S. Preibisch, C. Rueden, S. Saalfeld and B. Schmid, *Nature Methods*, 2012, 9, 676-682.
7. C. E. Walker, A. R. Taylor, G. Langer, G. M. Durak, S. Heath, I. Probert, T. Tyrrell, C. Brownlee and G. L. Wheeler, *New Phytologist*, 2018, 220, 147-162.
8. M. Andersson, C. Hem, L. Schultz, J. Nielsen, C. Pedersen, K. Sand, D. Okhrimenko, A. Johnsson and S. Stipp, *The Journal of Physical Chemistry A*, 2014, 118, 10720-10729.
9. A. Mucci, *Am. J. Sci*, 1983, 283, 780-799.
10. R. G. Compton and C. E. Banks, *Understanding voltammetry*, World Scientific, 2018.
11. P. Bobbert, M. Wind and J. Vlieger, *Physica A: Statistical Mechanics and its Applications*, 1987, 141, 58-72.
12. R. G. Compton, E. Laborda and K. R. Ward, *Understanding Voltammetry: Simulation Of Electrode Processes*, World Scientific Publishing Company, 2013.
13. C. Batchelor-McAuley and R. G. Compton, *Journal of Electroanalytical Chemistry*, 2020, 877, 114607.
14. R. D. Falgout and U. M. Yang, *hypre: A library of high performance preconditioners*, Springer, 2002.